Hindawi
Journal of Nanomaterials
Volume 2019, Article ID 6464713, 9 pages
https://doi.org/10.1155/2019/6464713

Research Article

Designing Carbon/Oxygen Ratios of Graphene Oxide Membranes for Proton Exchange Membrane Fuel Cells

Minwoo Ahn, Renlong Liu, Changgu Lee, and Wonyoung Lee

Department of Mechanical Engineering, Sungkyunkwan University, Republic of Korea

Correspondence should be addressed to Changgu Lee; peterlee@skku.edu and Wonyoung Lee; leewy@skku.edu

Received 15 September 2018; Revised 3 December 2018; Accepted 8 January 2019; Published 7 March 2019

Academic Editor: Vincenzo Baglio

Graphene oxide (GO), which is the oxidized form of graphene, has holes and functional groups on the surface and thus has high potential to be used as an electrochemical transport channel material. In this study, differently modified GO membranes are applied as electrolytes of proton exchange membrane fuel cells (PEMFCs) with controlled carbon/oxygen ratios. The critical and desired properties of the electrolyte, such as electron conductivity, proton conductivity, interfacial reactivity, and cell performance are evaluated in identical platinum-sputtered model electrodes. Among them, with the help of an increased concentration of oxygen-containing groups, a GO membrane with a low carbon/oxygen ratio shows a 2.9-fold improved maximum power density and advanced electrochemical properties compared with the pristine GO membrane. The characterization of GO suggests that the redox state of the membrane is an important factor for controlling the proton conductivity, interfacial reactivity, and maximum power density of PEMFCs.

1. Introduction

As a direct energy conversion device, the fuel cell is one of the most promising candidates for satisfying the increasing energy demand. Steady energy conversion, distributed generation, clean operation, and easy scaling are the typical merits of the fuel cell as a next-generation energy source [1–3]. Among the diverse types of fuel cells, the proton exchange membrane fuel cell (PEMFC) has been the most widely applied because of its suitable characteristics for efficient portable devices, including its dynamic characteristics (fast responsibility), durability (low operation below 100°C), and system compactness (minimized sealing issue). These features make the PEMFC the most competitive energy conversion source compared with other types of fuel cells and other energy conversion devices [4, 5].

Nafion is the most widely used electrolyte membrane for PEMFCs because of its high proton conductivity (>0.1 S/cm) and high water uptake rate (25.6 wt%) [6]. However, technical problems such as poor mechanical strength at elevated temperatures due to the low glass transition temperature (~110°C), fuel crossover requiring a minimum membrane thickness above a few tens of micrometers, and high cost are issues for Nafion-based PEMFCs [6–8]. To overcome these issues, there have been extensive efforts to develop Nafion-free materials, including ZrP, which contains zirconium phosphate anionic chains and NH_4^+ cations [9]; $Ti_3C_2T_x$-MXene-applied polybenzimidazole [10]; a polyvinyl alcohol and poly-urea-copolymer composite membrane [11]; and graphene oxide (GO) [12, 13]. Among these, GO is one of the most promising candidates owing to its relatively facile and cheap production process, remarkable mechanical stability with a high elastic modulus (GO: 680 ± 9.7 MPa and Nafion: 94.9 ± 8.5 MPa [6]), and fuel impermeability with a thickness of only 0.1 μm [14]. In addition, GO exhibits excellent water uptake with diverse functional groups, which is crucial for a high proton conductivity [15].

To exploit these advantages, studies on GO as an electrolyte of PEMFCs have focused on the external experimental conditions, involving modifications to the thickness of the membrane [7], operation temperature [6], operation humidity [16], and electrode structure [7]. Recently, the reduction effect of a GO membrane with photonic and thermal processes was reported, showing that the electrochemical

degradation as an electrolyte membrane, such as the increased electron conductivity and decreased proton conductivity, can cause a decreased open circuit voltage (OCV) and increased electrolyte membrane resistance, respectively [17]. A reduction study of GO is crucial as a fundamental approach for improving the cell performance by modifying the properties of the GO membrane. However, the insight into the application of GO as an electrolyte can be limited owing to the exclusion of the oxidation condition and performance evaluation. Moreover, from a fuel cell viewpoint, an undesirable increase in electron conductivity can degrade the cell performance, reducing the OCV. Despite the importance of fundamental insights into GO membranes, there have been few studies on GO with various oxidation states as an electrolyte of PEMFCs.

In this study, we fabricated GO membranes with different redox states by changing the carbon/oxygen ratios for the PEMFC electrolyte. We confirmed that the concentrations of oxygen-containing groups and sp^2-hybridized carbons were directly related to the proton and electron conductivity, respectively, according to the relationship between Fourier transform infrared (FT-IR) spectroscopy, X-ray photoelectron spectroscopy (XPS), and X-ray diffraction (XRD) analyses and water uptake measurements and electrochemical results. The GO cell with the lowest carbon/oxygen ratio showed a 2.9-fold improved maximum power density compared with the pristine GO cell, as well as enhanced proton conductivity and interfacial reactivity, because of the increased concentration of oxygen-containing groups.

2. Experiment Details

2.1. Synthesis of GO Solution. The Hummers method GO (GO (2.1), with a carbon : oxygen ratio of 2.1 : 1) solution was prepared from flake graphite (Alfa Aesar, -325 mesh) [18, 19] using the modified Hummers method. First, 30.7 g of H_2SO_4 was added to 0.5 g of graphite and 0.35 g of $NaNO_3$ with stirring in an ice-water bath, and then 1.95 g of $KMnO_4$ was added slowly to the suspension over 1 h. The mixture was stirred for another 2 h in the ice-water bath and for 1 d at room temperature. Then, 50 mL of water was added while the temperature was maintained at 98°C. The resultant mixture was further stirred for 1 h before it was cooled to the ambient temperature, and 1.5 mL of H_2O_2 (30 wt% aqueous solution) was slowly added. The mixture was purified with excess aqueous 5 wt% H_2SO_4/0.5 wt% H_2O_2 solution followed by deionized water 15 times. The resultant water solution was passed through a dialysis bag (Sigma-Aldrich) for 2 weeks until a pH of ~7 was reached. A stable and uniform GO (2.1) colloid suspension was then obtained via ultrasound sonication. $K_2S_2O_8$-induced highly oxidized GO (GO (1.5), with a carbon : oxygen ratio of 1.5 : 1) was prepared via the procedure proposed in our previous study [20], where modifications were made to the Hummers method. First, 0.5 g of graphite was placed in a flask, followed by the addition of 30.7 g of H_2SO_4 with stirring in an ice-water bath. Then, 4.5 g of $K_2S_2O_8$ was added to the as-prepared graphite suspension for preoxidization. The mixture was stirred for another 2 h in the ice-water bath and for 3-4 d at 35°C, following the same procedure used for the GO (2.1) synthesis.

2.2. Fabrication of Different GO Membranes. Both types of GO membranes were prepared by vacuum-filtering diluted GO dispersions through anodisc filter membranes with a pore size of 0.1 μm, followed by a 2 h vacuum heating process at 60°C under a vacuum of 50 mTorr. A low-temperature thermally reduced GO (GO (3.5), with a carbon : oxygen ratio of 3.5 : 1) membrane with a thickness of 10 μm was obtained via the thermal reduction of an 11.5 μm GO (2.1) membrane in air at 130°C for 1 h, owing to the shrinkage of the thickness of GO (2.1) after thermal reduction [21].

2.3. Fabrication of GO Cells. GO membranes were prepared in a square shape with dimensions of 1×1 cm^2 for a fuel cell application. Platinum electrodes were deposited on both sides of the GO membranes as model electrodes with an identical thickness of 100 nm using DC sputtering under an Ar background pressure of 75 mTorr and a plasma power of 100 W. The electrodes were patterned in a square shape with dimensions of 1×1 mm^2 by the shadow mask [22].

2.4. Characterization of GO Membranes. The chemical composition of the GO membranes was measured using XPS (K-Alpha, with an Al Ka μ-focused monochromator, 1,486.6 eV) and FT-IR spectroscopy (Bruker IFS-66/S, Tensor 27). The resistivity of the GO membranes was measured using a standardized four-point probe setup (Keithley model 2400 series) to eliminate the contact resistance. XRD measurements were performed using an HP thin-film X-ray diffractometer with Cu Ka radiation (1.5418 Å, 0.02° step^{-1}). The humidity during the XRD measurement and water uptake tests was controlled by using calibrated concentrated sulfuric acid with distilled water, which was placed at the bottom of the container in a small petri dish without any contact with the studied GO membranes. The concentrations of the sulfuric acid solution were 26.2% and 100%, yielding relative humidity (RH) values of 80% and 5%, respectively [20].

2.5. Electrochemical Measurement of GO Cells. For the electrochemical measurements, the GO cells were placed on a customized setup using silver paste (597-A, Aremco Products Inc.) as a current collector on the anode side and sealed with a ceramic adhesive (Ceramabond 552, Aremco Products Inc.). The GO cells were placed in a homemade water incubator overnight, at a constant temperature of 25°C and a constant RH of 80%, to supply sufficient humidity before measurement in the controlled chamber (TH-180S, Daeyang ETS Co. Ltd.). Electrochemical impedance spectroscopy (EIS) measurements were performed using an impedance analyzer (Gamry Reference 600, Gamry Instruments Inc.) in the frequency range of 10^{-2} to 10^6 Hz with an AC amplitude of 30 mV in the chamber. The 97% H_2-3% H_2O was supplied by the bubbler to the anode side at a flow rate of 100 sccm while the cathode was open to the air in the chamber. Calculations of area-specific resistance and proton conductivities of GO membranes were conducted as suggested in the supporting information.

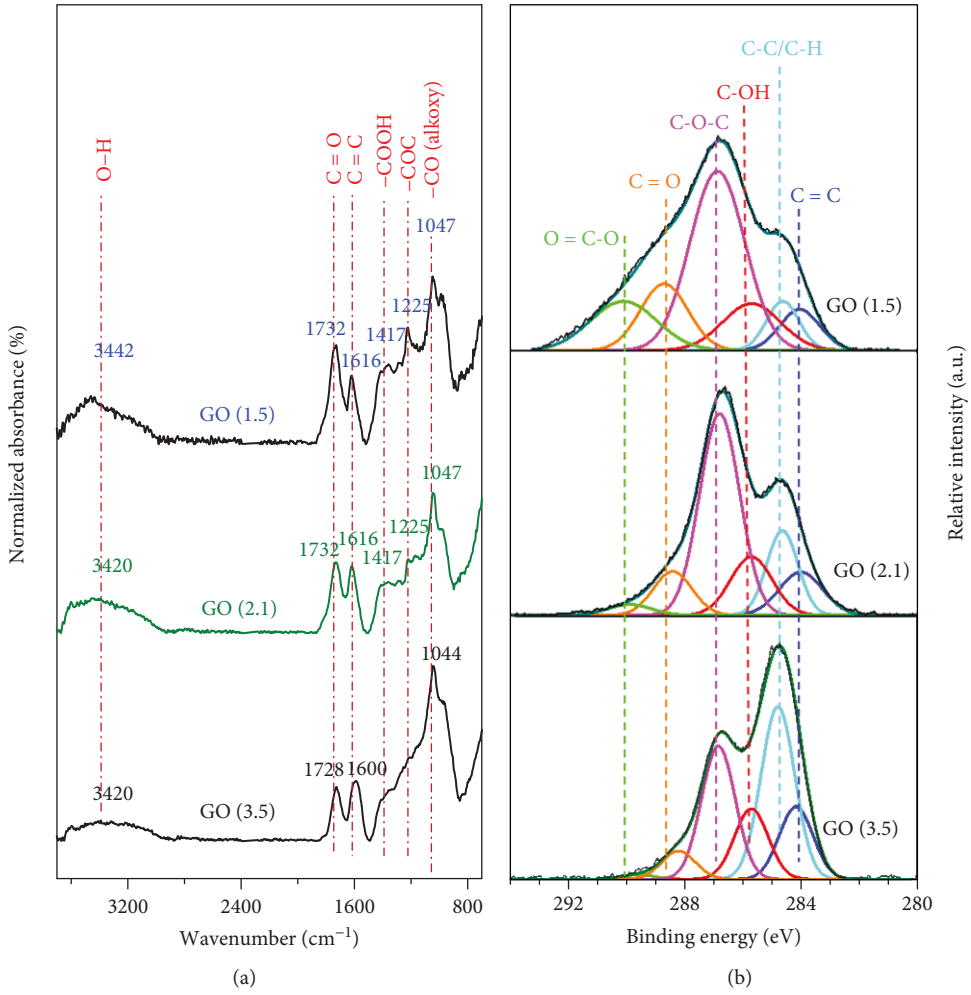

Figure 1: (a) FT-IR data and (b) high-resolution C1s XPS results for GO (1.5), GO (2.1), and GO (3.5) membranes.

3. Results and Discussion

3.1. Characterization of the GO Membranes. Three types of GO membranes with different carbon/oxygen ratios were fabricated separately to investigate the impacts of the functional groups on the proton and electron conductivities of the GO membranes. This is because the migration of protons and the proportion of free electrons in GO are determined by the water uptake of hydrophilic oxygen-containing groups and the content of sp^2 carbon bonds in GO, respectively. The presence and concentration differences of oxygen-containing functional groups in three types of GO were proven by FT-IR spectroscopy, as shown in Figure 1(a), and the following functional groups were identified: a broad, intense band of O–H stretching vibrations (3,420 cm^{-1}); narrower bands of C=O (carboxyl and carbonyl groups) stretching vibrations from carboxyl and carbonyl groups (1,720-1,740 cm^{-1}); C=C skeletal vibrations from unoxidized sp^2 CC bonds (1,600-1,620 cm^{-1}); O-H bending vibrations from hydroxyl groups (1,417 cm^{-1}); C–O–C vibrations (1,225 cm^{-1}); and a C-O (alkoxy) stretching peak at 1,047 cm^{-1} [23–25]. The intensities of the C=C bond stretching vibration of three different types of GO were normalized to the same value in order to compare the concentration ratio of C=O to C=C [26]. The ratio of C=O to C=C is 1.42, 1.02, and 0.87 for GO (1.5), GO (2.1), and GO (3.5), respectively. The intensity of the C=O stretching band at 1,732 cm^{-1} in GO (1.5) is the highest among all the types of GO, indicating a high concentration of carbonyl groups for GO (1.5). For GO (3.5), the intensities of the bands associated with oxygen-containing groups decreased or disappeared compared with those of unreduced GO. The effectiveness of the oxidation process of GO was evaluated according to the C/O ratios of GO [27]. To determine the specific contents of each functional group in GO, XPS was performed for a detailed elemental and chemical analysis, as shown in Figure 1(b). Figure 1(b) presents a typical C1s spectrum of three types of GO membranes, which is deconvoluted into six peaks that are attributed to different carbon bonds. The present XPS spectra consisting of C=C, C-C/C-H, C-OH, C(O)C, C=O, and O-C=O bonds were deconvoluted using the procedure proposed in our previous paper, and the result was in agreement with Liu et al. and Marcano et al. [20, 24]. The peaks appearing at 284.6 eV are attributed to

sp^3-hybridized C-C/C-H bonds, followed by a sp^2-hybridized C=C bond at 284.0 eV. Owing to the low content of these bonds in GO (2.1) and GO (1.5), the number of free electrons in these two types of GO is very low, in contrast with the dominant content of the sp^2 carbon bonding GO (3.5) and graphene [6, 28, 29]. The C-O-C epoxy groups at 286.8 eV are dominant species on the basal plane of GO. Hydroxyl C-OH at 285.7 eV, carbonyl C=O at 288.2 eV, and carboxyl groups at 289.9 eV are also present, with lower intensities, and are responsible for the strong binding to water via hydrogen bonds. The XPS results indicate that we successfully synthesized ultrahighly oxidized GO (1.5) with an unprecedented high content of carboxyl groups.

The content of each oxygenated functional group in different types of GO membranes is shown in Table 1. The group content data were obtained via integration to determine the area between the XPS peak data and the baseline, and the result is expressed as a percent of the total C1s peak area. In agreement with Figure 1(b), the contents of carbonyl groups (C=O bonds) are 5.8%, 9.9%, and 16.9%, respectively, with an increasing trend in the order of GO (3.5), GO (2.1), and GO (1.5), while the sp^2 C=C bonds and sp^3 C-C bonds exhibit the opposite trend. Because the carbon species (C-C and C-H) cannot contribute to electron conduction, as indicated by previous research [15, 30], the concentration of sp^2-hybridized carbon is italicized in Table 1, representing the electron conductivity of GO membranes. However, for each GO, the C=O to C=C ratio calculated via XPS does not perfectly match the concentration value in Figure 1(b). This is possibly because the resonance at 1,616 cm^{-1} in the FT-IR spectra can be assigned to the skeletal vibrations of unoxidized graphitic components but may also represent components from the adsorbed water molecules besides the ubiquitous O–H stretches that appear at 3,420 cm^{-1} as a broad and intense signal [31, 32]. Although the contents of hydroxyl groups (C-OH bonds) in GO (1.5) and GO (2.1) were comparable, the concentration of O-C=O bonds in GO (1.5) was approximately six times that in GO (2.1), indicating a significant increase in carboxyl groups when $K_2S_2O_8$ was added during the preoxidization process of GO (1.5) [33, 34]. Moreover, epoxy (C-O-C) and hydroxyl groups, which result in strong binding to water via hydrogen bonds, were the dominant species on the basal plane of GO (2.1). However, in GO (1.5), carbonyl groups (C=O and O-C=O) also account for a considerable share of the total groups, in addition to epoxy and hydroxyl groups. This indicates that the hydrophilicity of GO (1.5) has strong potential to be better than that of GO (2.1); thus, GO (1.5) has a higher water uptake value, which results in its better proton conductivity. By the comparison of the water contact angle of GO membranes, the trend of the hydrophilic property is made to coincide with our prediction as suggested in Figure S1 (wettability of GO membranes is GO (1.5)>GO (2.1)>GO (3.5)). In contrast, GO (3.5) fabricated via the thermal reduction process has smaller regions for oxygen-containing groups but larger electron-conductive sp^2 (C=C bonds) regions on the basal plane.

To investigate the water incubation mechanism in GO membranes, XRD analysis was performed to determine the interlayer distance of three types of GO membranes before and after water incubation. GO membranes with a thickness of 10 μm were exposed to two different water vapor pressures for 12 h and examined using XRD at an ambient temperature, as shown in Figure 2. The narrow peak of (001) reflection indicates that the interlayer distance between every two adjacent graphene flakes was uniform. Exposing the GO membranes to water vapor resulted in a shift of the (001) reflection, which corresponds to an increase in the interlayer distance. It can also be seen that as the water molecules interacted with the GO interlayers, the expansion of the corresponding GO membrane increased. The d-spacings, i.e., the interlayer distances, were calculated using Bragg's law: $\lambda = 2d \sin(\theta)$, where λ is the wavelength of the X-ray beam (0.154 nm), d is the distance between the adjacent GO flakes, and θ is the diffraction angle of the (001) peak. The spacing between the GO sheets in 80% RH for GO (1.5) was the largest among the GO membranes at up to 9.8 Å, which is 19.5% and 29.1% larger than those of the dry GO (1.5) membrane (8.2 Å) and the incubated GO (3.5) membrane (7.6 Å), respectively. Because GO (1.5) was the most oxidized GO membrane, before water incubation, it had the largest interlayer spacing, which allowed water molecules to easily permeate and diffuse along the nanocapillaries. This demonstrates that the increase of hydrophilic oxygen functional groups on GO membranes due to the increasing oxidation state enlarges the interlayer spacing of the GO membrane. When a portion of the functional groups on the GO (2.1) membranes was partially removed by thermal reduction, the typical peak near 11.5° (d-spacing ~7.7 Å) shifted to 12.7° (d-spacing ~6.9 Å), and a broader peak appeared at higher 2θ angles (23.5°; d-spacing ~3.8 Å), suggesting that the interlayer spacing of GO (2.1) decreased, forming GO (3.5), which has a more graphite-like structure than unreduced GO [35]. The expansion rates between the RH values of 5% and 80% for GO (1.5), GO (2.1), and GO (3.5) are calculated as 19.5%, 16.8%, and 10.1%, respectively, indicating that GO (1.5) has the largest water uptake capacity among the three kinds of GO membranes.

Water uptake measurements were performed separately using three types of GO membranes at the RH values of 5% and 80% to observe the influence of the GO oxidation on the water uptake capability. The water uptake rate (M) of GO was calculated as

$$M = \frac{m - m_{0d}}{m_{0d}} \times 100\,(\%), \tag{1}$$

where m is the mass of the GO membrane (with moisture), and m_{0d} is the mass of the GO membrane after vacuum oven drying at 60°C for 2 h (no moisture). The water uptake of GO (1.5) (45.9 wt%) was significantly higher than that of GO (2.1) (28.5 wt%) and GO (3.5) (20.2 wt%) owing to the larger amount of oxygen-containing groups in GO (1.5). Compared with the reported water uptake rate of the Nafion membrane (25.6 wt%) [6], the increased water uptake rates of GO (1.5) and GO (2.1) can contribute to efficient proton conduction,

Table 1: Area of each bonding peak in three types of GO, obtained via integration (%).

Fitted XPS area (%)		GO (1.5)	GO (2.1)	GO (3.5)
Carbon species	C-C/C-H	9.0	15.4	36.4
sp^2-hybridized carbon	C=C	*8.4*	*10.8*	*15.1*
	C-OH	12.0	14.2	14.3
	C-O-C	37.8	47.0	27.2
Oxygen-containing groups	C=O	16.9	9.9	5.8
	O-C=O	15.9	2.7	1.2
	Sum	82.6	73.8	48.5

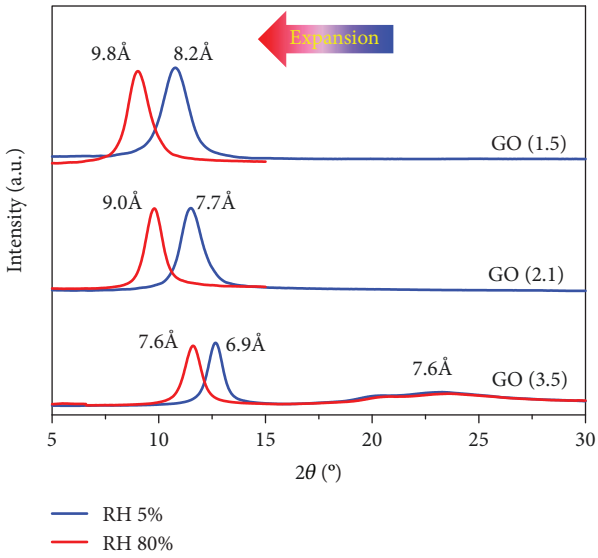

Figure 2: XRD patterns of GO (1.5), GO (2.1), and GO (3.5) at RH values of 5% and 80% for simulating the condition inside the GO proton exchange membrane before and after water incubation.

which is expected to improve with an increased level of hydration [36, 37]. Additionally, we checked the faster water uptake speed of GO (1.5) membranes for several lateral sizes and thicknesses compared to the commercial Nafion membrane as suggested in Figure S2. The higher water uptake rate of GO (1.5) compared with the other types of GO indicates a larger driving force for water absorption; that is, the GO (1.5) membrane may maintain its high proton conductivity even under low-humidity conditions.

Fabricated GO membranes were applied as electrolytes of a PEMFC with sputtered platinum electrodes. Figure 3(a) shows a schematic of the measurement setup, including a test jig as a support fixture, silver paste, and a gas-tight sealant. Figure 3(b) shows a cross-sectional scanning electron microscopy (SEM) image of a GO fuel cell with 100 nm thick platinum electrodes.

3.2. Electrochemical Results of the GO-Based Cells. Electrochemical measurements for fabricated GO cells with different carbon/oxygen ratios were conducted. As shown in Figure 4(a), Warburg resistances were observed for all the GO cells, which typically arise from the electrode reaction in room-temperature-operated PEMFCs [38] and form a divergent shape at a low frequency. The limitation of the maximum measurable frequency made the high-frequency loop unclear, especially for the GO (1.5) and GO (2.1) cells, owing to their low conduction resistance, as previously reported [6]. The GO (3.5) cell, which had a relatively high conduction resistance, exhibited a clear high-frequency loop. The x-intercept value of the high-frequency loop can be regarded as the proton conduction resistance [38, 39], which is the most important property of the electrolyte membrane. For the high-frequency loop, the GO (1.5), GO (2.1), and GO (3.5) cells showed area-specific resistance (ASR) values of 0.5, 4, and 20 Ωcm^2, respectively, which correspond to proton conductivities of 2×10^{-3}, 2.5×10^{-4}, and 5×10^{-5} S/cm, respectively. The measured proton conductivity of the GO (2.1) cell matches well with the previously reported values of 1.5-3 $\times 10^{-4}$ S/cm [6, 16]. The GO cell with the lowest carbon/oxygen ratio for GO (1.5) exhibited a substantially higher proton conductivity than the others. This trend of proton conductivity matches well with the characterization results for GO membranes with different redox states obtained using FT-IR, XPS, XRD, and water uptake characterizations. FT-IR analysis confirmed the existence of functional sp^2-hybridized carbon atoms and oxygen-containing groups in all the GO membranes. In more detail, quantitative XPS area fitting showed that the fraction of oxygen-containing groups, which represent possible water adsorption sites, decreased with the increase of the carbon/oxygen ratio: 82.6% for GO (1.5), 73.8% for GO (2.1), and 48.5% for GO (3.5). XRD analysis showed the direct interlayer expansion rate between dried (RH 5%) and humidified (RH 80%) conditions, indicating that the structural water adsorption capacity decreased with the increase of the carbon/oxygen ratio: 19.5% for GO (1.5), 16.8% for GO (2.1), and 10.1% for GO (3.5). The water uptake capacity, which can represent the absolute mass of adsorbed water, decreased with the increase of the carbon/oxygen ratio: 45.9 wt% for GO (1.5), 28.5 wt% for GO (2.1), and 20.2 wt% for GO (3.5). These water-related analyses and evaluations are crucial indicators of the shifted proton conductivity of the electrolyte membrane, according to the Grottuss mechanism [36, 37], which shows that proton conduction occurs as a structural diffusion through water content. Therefore, the lowest proton conduction resistance of GO (1.5) confirmed by EIS analysis compared well with the other GO membranes with lower carbon/oxygen ratios that stemmed from the

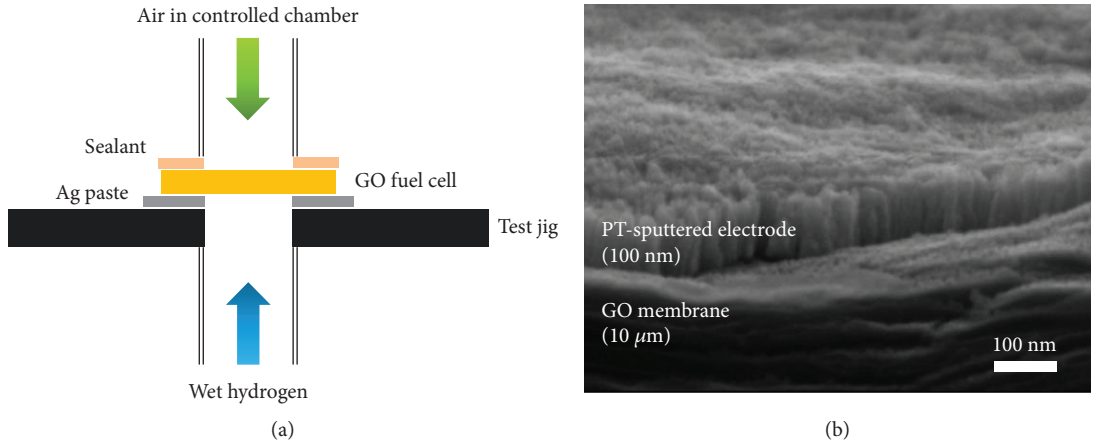

Figure 3: (a) Schematics for cell measurement and (b) cross-sectional SEM image of a GO fuel cell with a platinum electrode.

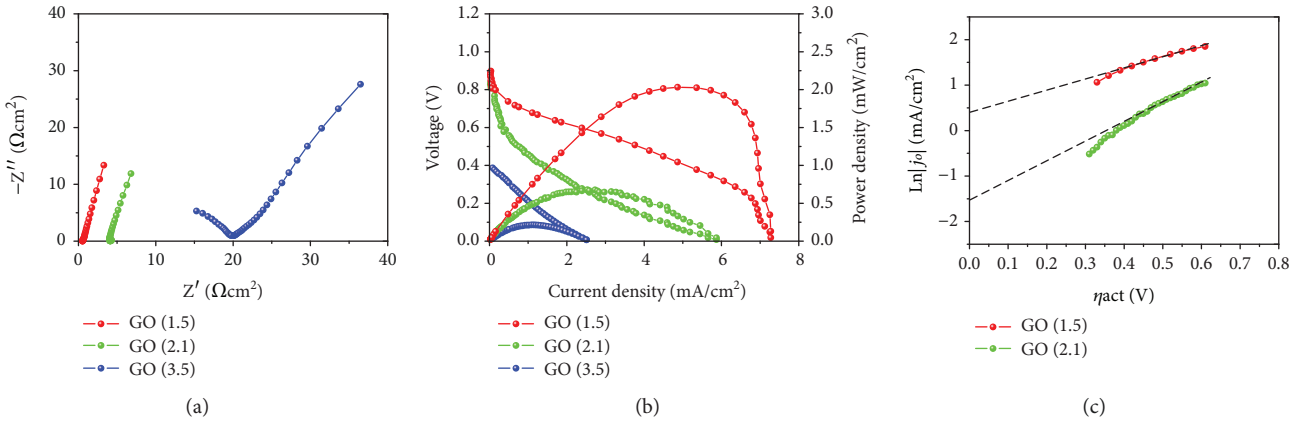

Figure 4: Electrochemical analysis for GO (1.5), GO (2.1), and GO (3.5) cells: (a) Nyquist plots, (b) I-V curves, and (c) Tafel plots.

larger amount of oxygen-containing groups and matched well with previous XPS analyses for different chemical concentrations, XRD analyses of the interlayer spacing, and water uptake measurements indicating the actual water uptake amount.

Figure 4(b) shows the I-V curves of three GO cells with different carbon/oxygen ratios. The OCV, i.e., the y-intercept at zero current density, was the highest for GO (1.5), followed by GO (2.1) and GO (3.5), with values of 0.89, 0.83, and 0.4 V, respectively. The maximum power densities were 2.1, 0.68, and 0.21 mW/cm^2 for the GO (1.5), GO (2.1), and GO (3.5) cells, respectively. The low OCV for GO (3.5) originated from the increased electron conductivity, as shown in Table S1, due to the higher concentration of sp^2-hybridized carbon atoms (Table 1), which resulted in current leakage through the electrolyte. The possible membrane fracture stemmed from the degraded mechanical properties of the reduced GO compared with the pristine condition, such as Young's modulus and ultimate tensile strength, which can decrease by factors of 10 and two, respectively, as confirmed in a previous report [40]. This can be another factor causing the decreased OCV. Moreover, the proton conductivity, which is related to the water uptake capability, decreased with a higher concentration of sp^2-hybridized carbon atoms, as shown in Figure 4(a). Both the increased electron conductivity and the decreased proton conductivity made the GO (3.5) an improper membrane type for PEMFC operation, deteriorating the cell performance compared with the pristine GO (2.1) cell. On the other hand, the GO (1.5) cell showed the highest maximum power density, which was 2.9 times higher than that of the GO (2.1) cell, owing to the increased proton conductivity and OCV. The improved proton conductivity was deduced from the enhanced concentration of oxygen-containing groups, as shown in Table 1, and confirmed by the Nyquist plots in Figure 4(a). The slightly increased OCV of GO (1.5) compared with the pristine GO (2.1) cell stemmed from the decreased concentration of sp^2-hybridized carbon atoms (C=C), as shown in Table 1, and the increased electron resistivity, as shown in Table S1, which affected the electron conductivity.

Because the GO (3.5) cell showed significantly decreased performance, Tafel plots were only applied for the GO (1.5) and GO (2.1) cells, as shown in Figure 4(c), to compare the exchange current density values. The exchange current density (j_o), which is defined as the exchange rate between the reactant and product at equilibrium states, can represent the reactivity, including both the bulk electrode and the interfacial reaction [41]. Because identical platinum electrodes

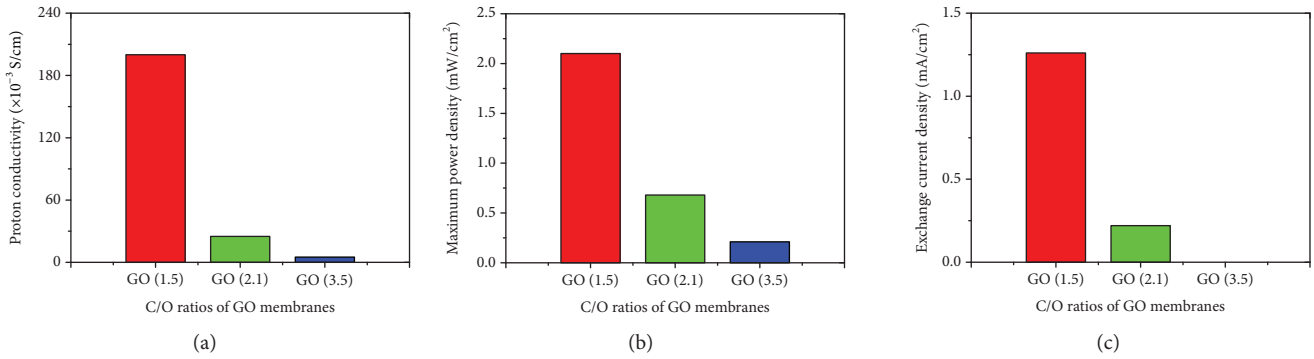

FIGURE 5: Electrochemical properties of GO cells with different C/O ratios: (a) proton conductivity, (b) maximum power density, and (c) exchange current density.

were used for all the GO cells, the exchange current density can be regarded as the interfacial reactivity of the GO membrane. For a detailed assessment of the interfacial reaction kinetics, the exchange current densities were calculated using the y-intercept values via the Tafel equation [42–44]:

$$\eta_{\text{act, cathode}} = \left(\frac{RT}{\alpha n F}\right) \cdot \ln\left(\frac{j}{j_o}\right), \tag{2}$$

where R is the ideal gas constant, T is the temperature, n is the number of moles of electrons transferred, F is Faraday's constant, α is the charge-transfer coefficient, j is the current density, and j_o is the exchange current density. A higher value of j_o can represent a more active oxygen reduction reaction at the cathode. As shown in Figure 4(c), the exchange current densities are 1.26 and 0.22 mA/cm^2 for the GO (1.5) and GO (2.1) cells, respectively. The cathode reaction, which is the dominant cause of electrode losses at triple-phase boundaries, can be expressed as follows:

$$\frac{1}{2}O_2 + 2e^- + 2H^+ \rightarrow H_2O \tag{3}$$

As shown in the above cathode reaction, oxygen gas, electrons, and protons are needed reactants, and if the number of reactants increases, the forward reaction generating the water in the cathode reaction and the electricity in the total reaction is activated. When the GO membrane is oxidized from GO (2.1) to GO (1.5), the higher concentration of oxygen-containing groups increases the proton conductivity, as shown in Figure 4(a) with the ASR change from 4 to 0.5 Ωcm^2. The enhanced proton conductivity of the GO (1.5) cell contributes to a faster provision of reactants and expedites the forward cathode reaction, yielding interfacial reactivity 5.7 times higher than that of the GO (2.1) cell. Together with the enhanced proton conductivity of the GO (1.5) cell, the improved interfacial reactivity is another factor causing the 2.9-fold performance increase, which shows the importance of membrane design.

3.3. Discussion. Figure 5 shows the electrochemical properties determined via EIS and I-V measurements with respect to the carbon/oxygen ratio. The proton and electron conductivities of differently treated GO membranes were confirmed by FT-IR and XPS analysis with the changes of the concentrations of oxygen-containing groups and sp^2-hybridized carbon, which can affect the conduction properties. These changes were evaluated using Nyquist plots and the four-point probe method. The interfacial reactivity of possible candidates can be analyzed according to the exchange current density of the Tafel plot. With the contributions of the modified conductivity and reactivity obtained via carbon/oxygen ratio control, the resultant maximum power density of the GO-based fuel cells was enhanced 2.9-fold. By comparing the cells with intermediate (GO (2.1)) and low (GO (1.5)) carbon/oxygen ratios, various analyses were performed, revealing an increase in the concentration of oxygen-containing groups from 73.8% to 82.6%, an increase in the water uptake rate from 28.5 to 45.9 wt%, and an increase in the interlayer spacing from 7.6 to 9.8 Å in the 80% RH condition. These confirmed structural advantages with carbon/oxygen control enhanced the proton conductivity by 5×10^{-5}, 2.5×10^{-4}, and 2×10^{-3} S/cm with respect to each redox state, as shown in Figure 5(a). The enhanced proton conductivity of the GO (1.5) cell can contribute to the 2.9-fold increase in the maximum power density, as shown in Figure 5(b). However, in the case of the GO (3.5) cell, the improved electron conductivity confirmed by four-point probing and the decreased proton conductivity confirmed by the Nyquist plot cause a significant OCV drop and increased membrane resistance, respectively, yielding 70% lower cell performance compared with GO (2.1). Additionally, by comparing the exchange current density representing the interfacial reactivity, we find another superior property of the lower carbon/oxygen ratio cell: a 5.7-fold enhancement in the exchange current density with the smooth provision of the reactant, as shown in Figure 5(c).

These results agree with the FT-IR, XPS, and XRD analyses and water uptake measurements, indicating the importance of electrolyte engineering not only for the bulk conductivity, but also for the interfacial reactivity between the electrolyte and the electrode. Regarding the conductivity, we can confirm that the proton conductivity and electron conductivity are inversely proportional to the carbon/oxygen ratio and the redox state of the GO membrane. Regarding the

interfacial reactivity, the lower carbon/oxygen ratio cells showed an improved exchange current density compared with the pristine cell, with faster provision of protons for the oxygen reduction reaction at the cathodes. The lower carbon/oxygen ratio cell is more desirable than the pristine cell for PEMFC operation and demonstrates advanced electrochemical properties and enhanced performance with modified oxygen-containing groups for both conduction and reaction.

4. Conclusions

GO membranes with different carbon/oxygen ratios were systematically tested to investigate their potential as an electrolyte of PEMFCs. The carbon/oxygen ratios were successfully designed via thermal reduction and solution-based oxidation processes. For the lower carbon/oxygen ratio GO cell, the following electrochemical properties could be efficiently designed: (1) an increased OCV with a decreased concentration of sp^2-hybridized carbon atoms, (2) an increased proton conductivity with an increased concentration of oxygen-containing groups, and (3) an increased interfacial reactivity due to the enforced forward electrode reaction. Both the proton/electron conductivities and the interfacial reactivity were effectively modified through the electrolyte design, yielding efficient PEMFCs that exhibited a 2.9-fold enhanced maximum power density. Our results shed light on designing the electrolyte structure with consideration of both the conductivities and the interfacial reactivity for achieving high-performing PEMFCs.

Data Availability

The data used to support the findings of this study are included within the article and in the file provided in the Supplementary Materials.

Conflicts of Interest

The authors declare that they have no conflicts of interest.

Authors' Contributions

Minwoo Ahn and Renlong Liu contributed equally to this work.

Acknowledgments

This research was supported by the Basic Science Research Program through the National Research Foundation of Korea (NRF), which is funded by the Ministry of Science, ICT, & Future Planning (Grant Nos. NRF-2016R1C1 B2011289 and NRF-2016R1A2B4012931); the Korea Institute of Energy Technology Evaluation and Planning (KETEP); and the Ministry of Trade, Industry, and Energy, Republic of Korea (MOTIE) (No. 20173010032170).

Supplementary Materials

Supporting information is composed of four parts: (1) Electrical conductivity measurement of GO membranes: this measurement was conducted to confirm the electrical conductivity. By comparing the conductivity of the membranes, the measured open circuit voltages (OCV) of GO cells in the main manuscript could be double-checked. Especially, the drastically decreased OCV value of the GO (3.5) membrane can be well explained. (2) Contact angle measurement of GO membranes: according to the review's request, we checked the contact angles of GO membranes to confirm the different hydrophilic properties of the GO (1.5) membrane compared to other GO membranes. (3) Water uptake rate with respect to time: according to the reviewer's request, we measured the water adsorption trend of GO membranes which can be one of the important parameters of GO membranes as the electrolyte of PEMFCs. (4) Calculation of area-specific resistance and proton conductivity: discussed in detail in the electrochemical analysis part of the paper. *(Supplementary Materials)*

References

[1] E. D. Wachsman and K. T. Lee, "Lowering the temperature of solid oxide fuel cells," *Science*, vol. 334, no. 6058, pp. 935–939, 2011.

[2] M. Winter and R. J. Brodd, "What are batteries, fuel cells, and supercapacitors?," *Chemical Reviews*, vol. 104, no. 10, pp. 4245–4269, 2004.

[3] M. Ahn, J. Lee, and W. Lee, "Nanofiber-based composite cathodes for intermediate temperature solid oxide fuel cells," *Journal of Power Sources*, vol. 353, pp. 176–182, 2017.

[4] Y. Wang, K. S. Chen, J. Mishler, S. C. Cho, and X. C. Adroher, "A review of polymer electrolyte membrane fuel cells: technology, applications, and needs on fundamental research," *Applied Energy*, vol. 88, no. 4, pp. 981–1007, 2011.

[5] S. Litster and G. McLean, "PEM fuel cell electrodes," *Journal of Power Sources*, vol. 130, no. 1-2, pp. 61–76, 2004.

[6] T. Bayer, S. R. Bishop, M. Nishihara, K. Sasaki, and S. M. Lyth, "Characterization of a graphene oxide membrane fuel cell," *Journal of Power Sources*, vol. 272, pp. 239–247, 2014.

[7] H. Tateishi, K. Hatakeyama, C. Ogata et al., "Graphene oxide fuel cell," *Journal of the Electrochemical Society*, vol. 160, no. 11, pp. F1175–F1178, 2013.

[8] Q. Li, R. He, J. O. Jensen, and N. J. Bjerrum, "Approaches and recent development of polymer electrolyte membranes for fuel cells operating above 100 °C," *Chemistry of Materials*, vol. 15, no. 26, pp. 4896–4915, 2003.

[9] D. Gui, X. Dai, Z. Tao et al., "Unique proton transportation pathway in a robust inorganic coordination polymer leading to intrinsically high and sustainable anhydrous proton conductivity," *Journal of the American Chemical Society*, vol. 140, no. 19, pp. 6146–6155, 2018.

[10] M. Fei, R. Lin, Y. Deng et al., "Polybenzimidazole/Mxene composite membranes for intermediate temperature polymer electrolyte membrane fuel cells," *Nanotechnology*, vol. 29, no. 3, article 035403, 2018.

[11] T. Zhou, B. Ao, Y. Wei, S. Chen, K. Lian, and J. Qiao, "Fabricating hydroxyl anion conducting membranes based on poly(vinyl alcohol) and bis(2-chloroethyl) ether-1,3-bis(3-

(dimethylamino)propyl) urea copolymer with linear anion-exchange sites for polymer electrolyte membrane fuel cell," *Solid State Ionics*, vol. 308, pp. 112–120, 2017.

[12] X. He, G. He, A. Zhao et al., "Facilitating proton transport in nafion-based membranes at low humidity by incorporating multifunctional graphene oxide nanosheets," *ACS Applied Materials & Interfaces*, vol. 9, no. 33, pp. 27676–27687, 2017.

[13] M. Vinothkannan, A. R. Kim, G. Gnana kumar, and D. J. Yoo, "Sulfonated graphene oxide/Nafion composite membranes for high temperature and low humidity proton exchange membrane fuel cells," *RSC Advances*, vol. 8, no. 14, pp. 7494–7508, 2018.

[14] R. R. Nair, H. A. Wu, P. N. Jayaram, I. V. Grigorieva, and A. K. Geim, "Unimpeded permeation of water through helium-leak-tight graphene-based membranes," *Science*, vol. 335, no. 6067, pp. 442–444, 2012.

[15] M. R. Karim, K. Hatakeyama, T. Matsui et al., "Graphene oxide nanosheet with high proton conductivity," *Journal of the American Chemical Society*, vol. 135, no. 22, pp. 8097–8100, 2013.

[16] K. Hatakeyama, M. R. Karim, C. Ogata et al., "Proton conductivities of graphene oxide nanosheets: single, multilayer, and modified nanosheets," *Angewandte Chemie International Edition*, vol. 53, no. 27, pp. 6997–7000, 2014.

[17] K. Hatakeyama, H. Tateishi, T. Taniguchi et al., "Tunable graphene oxide proton/electron mixed conductor that functions at room temperature," *Chemistry of Materials*, vol. 26, no. 19, pp. 5598–5604, 2014.

[18] W. S. Hummers Jr and R. E. Offeman, "Preparation of graphitic oxide," *Journal of the American Chemical Society*, vol. 80, no. 6, pp. 1339–1339, 1958.

[19] R. Liu, G. Arabale, J. Kim et al., "Graphene oxide membrane for liquid phase organic molecular separation," *Carbon*, vol. 77, pp. 933–938, 2014.

[20] R. Liu, T. Gong, K. Zhang, and C. Lee, "Graphene oxide papers with high water adsorption capacity for air dehumidification," *Scientific Reports*, vol. 7, no. 1, Article 9761, 2017.

[21] S. Pei, J. Zhao, J. Du, W. Ren, and H.-M. Cheng, "Direct reduction of graphene oxide films into highly conductive and flexible graphene films by hydrohalic acids," *Carbon*, vol. 48, no. 15, pp. 4466–4474, 2010.

[22] J. Y. Koo, Y. Lim, Y. B. Kim, D. Byun, and W. Lee, "Electrospun yttria-stabilized zirconia nanofibers for low-temperature solid oxide fuel cells," *International Journal of Hydrogen Energy*, vol. 42, no. 24, pp. 15903–15907, 2017.

[23] J. Zhang, H. Yang, G. Shen, P. Cheng, J. Zhang, and S. Guo, "Reduction of graphene oxide vial-ascorbic acid," *Chemical Communications*, vol. 46, no. 7, pp. 1112–1114, 2010.

[24] D. C. Marcano, D. V. Kosynkin, J. M. Berlin et al., "Improved synthesis of graphene oxide," *ACS Nano*, vol. 4, no. 8, pp. 4806–4814, 2010.

[25] M. J. Fernandez-Merino, L. Guardia, J. I. Paredes et al., "Vitamin C is an ideal substitute for hydrazine in the reduction of graphene oxide suspensions," *Journal of Physical Chemistry C*, vol. 114, no. 14, pp. 6426–6432, 2010.

[26] D. Calloway, "Beer-Lambert Law," *Journal of Chemical Education*, vol. 74, no. 7, pp. 744–744, 1997.

[27] D. R. Dreyer, S. Park, C. W. Bielawski, and R. S. Ruoff, "The chemistry of graphene oxide," *Chemical Society Reviews*, vol. 39, no. 1, pp. 228–240, 2010.

[28] R. Haerle, E. Riedo, A. Pasquarello, and A. Baldereschi, "sp^2/sp^3 hybridization ratio in amorphous carbon from C1s core-level shifts: X-ray photoelectron spectroscopy and first-principles calculation," *Physical Review B*, vol. 65, no. 4, 2001.

[29] H. Estrade-Szwarckopf, "XPS photoemission in carbonaceous materials: a "defect" peak beside the graphitic asymmetric peak," *Carbon*, vol. 42, no. 8-9, pp. 1713–1721, 2004.

[30] V. B. Mohan, R. Brown, K. Jayaraman, and D. Bhattacharyya, "Characterisation of reduced graphene oxide: effects of reduction variables on electrical conductivity," *Materials Science and Engineering: B*, vol. 193, pp. 49–60, 2015.

[31] S. Stankovich, R. D. Piner, S. T. Nguyen, and R. S. Ruoff, "Synthesis and exfoliation of isocyanate-treated graphene oxide nanoplatelets," *Carbon*, vol. 44, no. 15, pp. 3342–3347, 2006.

[32] T. Szabo, O. Berkesi, and I. Dekany, "DRIFT study of deuterium-exchanged graphite oxide," *Carbon*, vol. 43, no. 15, pp. 3186–3189, 2005.

[33] G. Eda, G. Fanchini, and M. Chhowalla, "Large-area ultrathin films of reduced graphene oxide as a transparent and flexible electronic material," *Nature Nanotechnology*, vol. 3, no. 5, pp. 270–274, 2008.

[34] H. K. Jeong, H. J. Noh, J. Y. Kim, M. H. Jin, C. Y. Park, and Y. H. Lee, "X-ray absorption spectroscopy of graphite oxide," *EPL (Europhysics Letters)*, vol. 82, no. 6, article 67004, 2008.

[35] I. K. Moon, J. Lee, R. S. Ruoff, and H. Lee, "Reduced graphene oxide by chemical graphitization," *Nature Communications*, vol. 1, no. 6, pp. 1–6, 2010.

[36] K. D. Kreuer, S. J. Paddison, E. Spohr, and M. Schuster, "Transport in proton conductors for fuel-cell applications: simulations, elementary reactions, and phenomenology," *Chemical Reviews*, vol. 104, no. 10, pp. 4637–4678, 2004.

[37] N. Agmon, "The Grotthuss mechanism," *Chemical Physics Letters*, vol. 244, no. 5-6, pp. 456–462, 1995.

[38] S. Mikhailenko, M. Guiver, and S. Kaliaguine, "Measurements of PEM conductivity by impedance spectroscopy," *Solid State Ionics*, vol. 179, no. 17-18, pp. 619–624, 2008.

[39] T. J. Freire and E. R. Gonzalez, "Measurements of PEM conductivity by impedance spectroscopy," *Journal of Electroanalytical Chemistry*, vol. 503, no. 1-2, pp. 57–68, 2001.

[40] O. C. Compton and S. T. Nguyen, "Graphene oxide, highly reduced graphene oxide, and graphene: versatile building blocks for carbon-based materials," *Small*, vol. 6, no. 6, pp. 711–723, 2010.

[41] R. O'Hayre, S.-W. Cha, W. Colella, and F. B. Prinz, *Fuel Cell Fundamentals*, John Wiley & Sons, 2016.

[42] M. Choi, J. Y. Koo, M. Ahn, and W. Lee, "Effects of grain boundaries at the electrolyte/cathode interfaces on oxygen reduction reaction kinetics of solid oxide fuel cells," *Bulletin of the Korean Chemical Society*, vol. 38, no. 4, pp. 423–428, 2017.

[43] Y. B. Kim, J. S. Park, T. M. Gür, and F. B. Prinz, "Oxygen activation over engineered surface grains on YDC/YSZ interlayered composite electrolyte for LT-SOFC," *Journal of Power Sources*, vol. 196, no. 24, pp. 10550–10555, 2011.

[44] J. H. Shim, C.-C. Chao, H. Huang, and F. B. Prinz, "Atomic layer deposition of yttria-stabilized zirconia for solid oxide fuel cells," *Chemistry of Materials*, vol. 19, no. 15, pp. 3850–3854, 2007.